Cross Entropy Benchmark for Measurement-Induced Phase Transitions

Yaodong Li,[1,2] Yijian Zou,[2] Paolo Glorioso,[2] Ehud Altman,[3] and Matthew P. A. Fisher[1]

[1] *Department of Physics, University of California, Santa Barbara, CA 93106*
[2] *Department of Physics, Stanford University, Stanford, CA 94305*
[3] *Department of Physics, University of California, Berkeley, CA 94720*

(Dated: August 27, 2022)

We investigate the prospects of employing the linear cross-entropy to experimentally access measurement-induced phase transitions (MIPT) without requiring any postselection of quantum trajectories. For two random circuits that are identical in the bulk but with different initial states, the linear cross-entropy χ between the bulk measurement outcome distributions in the two circuits acts as a boundary order parameter, and can be used to distinguish the volume law from area law phases. In the volume law phase (and in the thermodynamic limit) the bulk measurements cannot distinguish between the two different initial states, and $\chi = 1$. In the area law phase $\chi < 1$. For circuits with Clifford gates, we provide numerical evidence that χ can be sampled to accuracy ε from $O(1/\varepsilon^2)$ trajectories, by running the first circuit on a quantum simulator *without postselection*, aided by a classical simulation of the second. We also find that for weak depolarizing noise the signature of the MIPT is still present for intermediate system sizes. In our protocol we have the freedom of choosing initial states such that the "classical" side can be simulated efficiently, while simulating the "quantum" side is still classically hard.

I. INTRODUCTION

Open quantum dynamics can host a rich phenomenology, including a family of measurement-induced phase transitions (MIPT) in the scaling of entanglement along quantum trajectories in monitored systems [1–7]. While the MIPT occurs generically in a number of different models [8–26], its verification can be challenging even on an error-corrected quantum computer, due to the so-called "postselection problem". Quantum trajectories are labeled by the measurement history $\mathbf{m}$, whose length is extensive in the space-time volume V of the circuit; thus, the number of possible trajectories $\mathbf{m}$ is exponential in V, but they each occur with roughly the same probability. On the other hand, one needs multiple copies of the same $\mathbf{m}$ in order to verify any quantum entanglement; and then many different $\mathbf{m}$ to perform a proper statistical average. On a quantum simulator there is no general recipe for producing such copies other than running the quantum circuit many times and waiting until the measurement results coincide ("postselection"). In other words, the prepration of the output state is not readily "repeatable", and naively $O(e^V)$ runs of the circuit are required to generate multiple copies, thus severely restricting the scalability of such experiments. Nevertheless, in an impressive recent experiment that carries out postselection [27], the MIPT is observed on small scale superconducting quantum processors.

The exponential postselection overhead has been shown to be avoidable in two cases. First, when only Clifford circuits are considered, the entanglement can be verified by "decoding" the circuit, either through a full classical simulation within the stabilizer formalism [28] or via machine learning [29]. With machine learning the authors claim that "decoding" is possbile also beyond Clifford circuits, although this has yet to be explored in detail. Second, when the non-unitary (monitored) dynamics is a spacetime dual of a unitary one [30–32], postselection is partially ameliorated, and correspondences between unitary dynamics and monitored dynamics can be made.[1]

Here we propose a resource efficient experimental protocol for verifying the MIPT in random circuits, by estimating the "linear cross-entropy" (denoted χ) between the probability distribution of (bulk circuit) measurement outcomes $\mathbf{m}$ in two circuits with the same bulk but different initial states, ρ and σ. A closely related quantity has been discussed by Bao *et. al.* [7], and in Ref. [34]. In particular, as we establish both numerically and analytically, in the thermodynamic limit the linear cross-entropy (when suitably normalized) is 1 in the volume law phase, and equals a nonuniversal constant smaller than 1 in the area law phase. Thus, the MIPT can also be viewed as a phase transition in the distinguishability of two initial states, when the bulk measurement outcomes are given. Indeed, the MIPT is a transition in the bulk structure of the quantum circuit, where the scaling of the entanglement entropy in the output state is just one of its many ramifications. A full appreciation of this fact may lead to other ways of probing the transition experimentally.

The definition of χ includes contributions from all samples of $\mathbf{m}$, and to estimate χ no postselection is involved. However, as we discuss below (see Sec. II), estimating χ usually requires an exponentially long classical simulation, thus not scalable. In Sec. II B, we show that the classical simulation becomes scalable in Clifford ciruits, where χ can be efficiently sampled by running the ρ-circuit on a quantum simulator, aided by a classical simulation of the σ-circuit. For a fixed circuit we estimate

[1] We bring the reader's attention to a recent proposal of revealing the MIPT using "pre-selection" [33].

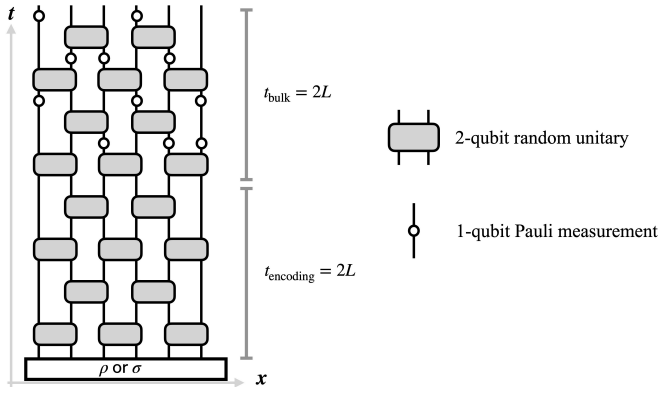

FIG. 1. The layout of the hybrid circuit considered in this paper. Different from the usual setup [9], we have an additional "encoding" stage before the hybrid evolution for time $t_{\text{encoding}} = 2L$, following Ref. [5]. We call the evolution after the encoding stage the "circuit bulk", which last for another $t_{\text{bulk}} = 2L$. The total circuit time is $T = t_{\text{encoding}} + t_{\text{bulk}} = 4L$. We will compare two different initial states ρ and σ (left unspecified for the moment) undergoing the same circuit evolution.

that the number of samples of $\mathbf{m}$ scales as $1/\varepsilon^2$. We provide numerical evidence that χ is an order parameter for the MIPT (i.e. $\chi = 1$ in the volume law phase and $\chi < 1$ in the area law phase), and simulate the effect of depolarizing noise. We find that depolarizing noise generically decreases χ regardless of p, and in the thermodynamic limit we expect no transition for any finite noise rate.

By choosing the circuit bulk to be composed of Clifford operations and σ to be a stabilizer state, the protocol is scalable on both the quantum and the classical sides. Nevertheless, unless ρ is also a stabilizer state, the ρ-circuit output state is still highly nontrivial and hard to represent classically. In Appendix C, we consider one nontrivial aspect of the output state in the volume law phase, and show that with a generic (nonstabilizer) choice of ρ the probability distribution over the output bitstrings obeys a nontrivial distribution with a long tail, similar to, but different in detail than, the Porter-Thomas distribution from purely unitary random circuits. We discuss possible implications of this result.

II. LINEAR CROSS-ENTROPY AND ORDER PARAMETER

We consider the "hybrid" circuit shown in Fig. 1, composed of both unitary gates on nearest-neighbor qubits arranged in a brickwork structure, and single-site measurements in the bulk, performed with probability p at each qubit within each time step. By convention, each time step contains $L/2$ unitary gates. Different from the usual setup [9], we have an additional "encoding" stage before the hybrid evolution for time $t_{\text{encoding}} = 2L$, following Ref. [5]. The reason for this somewhat unusual choice is practical, to get a clearer experimental signal of the MIPT; see Sec. II C. We call the evolution after the encoding stage the "circuit bulk", which lasts for another $t_{\text{bulk}} = 2L$. The total circuit time is $T = t_{\text{encoding}} + t_{\text{bulk}} = 4L$.

For concreteness, we take all the measurements to be in the Pauli Z basis. Given a circuit layout (as determined by the brickwork structure and the location of measurements) and the unitary gates in the bulk – which we denote collectively as C – the *unnormalized* output state is defined by C and the measurement record $\mathbf{m} = \{m_1, m_2, \ldots, m_N\}$ as

$$\rho_{\mathbf{m}} = C_{\mathbf{m}} \rho C_{\mathbf{m}}^\dagger, \tag{1}$$

where $C_{\mathbf{m}}$ is the time-ordered product of all the unitaries and projectors in the circuit, written schematically as

$$\begin{aligned} C_{\mathbf{m}} = {} & P_{m_N} P_{m_{N-1}} \ldots P_{m_{N-N_T+1}} \cdot U_T \\ & \cdot P_{m_{N-N_T}} \ldots P_{m_{N-N_T-N_{T-1}+1}} \cdot U_{T-1} \\ & \cdot P_{m_{N-N_T-N_{T-1}}} \ldots P_{m_{N-N_T-N_{T-1}-N_{T-2}+1}} \cdot U_{T-2} \\ & \ldots \end{aligned} \tag{2}$$

Here each line contains all quantum operations in one circuit time step, and N is the total number of measurements, which is proportional to the spacetime volume of the circuit, $N \propto pV = pLT$. The corresponding probability of obtaining $\mathbf{m}$ is given by

$$p_{\mathbf{m}}^\rho = \operatorname{tr} \rho_{\mathbf{m}}. \tag{3}$$

We define similar quantities for a different initial state σ,

$$\sigma_{\mathbf{m}} = C_{\mathbf{m}} \sigma C_{\mathbf{m}}^\dagger, \tag{4}$$

$$p_{\mathbf{m}}^\sigma = \operatorname{tr} \sigma_{\mathbf{m}}. \tag{5}$$

With these, we define the (normalized) linear cross-entropy of the circuit between the two initial states as

$$\chi_C = \frac{\sum_{\mathbf{m}} p_{\mathbf{m}}^\rho p_{\mathbf{m}}^\sigma}{\sum_{\mathbf{m}} \left(p_{\mathbf{m}}^\sigma\right)^2}. \tag{6}$$

Here, after averaging over $\mathbf{m}$, χ_C only depends on the circuit C, and we have explicitly included this dependence in our notation. Finally, we take its average over C,

$$\chi := \mathbb{E}_C \chi_C = \mathbb{E}_C \frac{\sum_{\mathbf{m}} p_{\mathbf{m}}^\rho p_{\mathbf{m}}^\sigma}{\sum_{\mathbf{m}} \left(p_{\mathbf{m}}^\sigma\right)^2}. \tag{7}$$

It was previously pointed out [7] that a quantity closely related to $-\ln \chi$ corresponds to the free energy cost after fixing a boundary condition in a (replicated) spin model [6, 7, 35, 36]; in Appendix A we provide a similar calculation for our circuit. From this derivation we expect $1-\chi = e^{-O(L)}$ for large L in the volume law phase ($p < p_c$), and $1 - \chi > 0$ in the area law phase ($p > p_c$), even as $L \to \infty$.

The physical meaning of χ should be clear: it quantifies the difference between the probability distributions

over measurement histories for the two initial states. In the volume law phase, $\chi = 1$ implies the impossibility of distinguishing different initial states from bulk measurements, due to the "coding" properties of this phase (i.e. the dynamics in the volume law phase generates a "dynamical quantum memory" [4, 5, 37–40]). In particular, in the volume law phase, local measurements are so infrequent that it extracts little information about the inital state, as the information is sufficiently scrambled by the random unitaries. The code breaks down when p is increased past the transition, and χ saturates to a finite, nonuniversal constant strictly smaller than 1. In this phase, information about the initial state leaks into the measurement outcomes.

We now briefly outline a protocol for estimating χ, which is similar to the linear cross-entropy benchmark ("linear XEB") for random unitary circuits [41, 42]. Then we discuss its limitations when applied to the MIPT and how to overcome them in case of a stabilizer circuit.

A. General setup

Consider running the circuit with initial state ρ ("the ρ-circuit") on a quantum simulator. From the simulation we obtain a measurement record $\mathbf{m}$, an event that occurs with probability $p^\rho_{\mathbf{m}}$. Given $\mathbf{m}$ we can perform a classical simulation with the initial state σ, and calculate the corresponding probablity $p^\sigma_{\mathbf{m}}$. Repeating this M times, we obtain a sequence of probabilities $\{p^\sigma_{\mathbf{m}_1}, p^\sigma_{\mathbf{m}_2}, \dots p^\sigma_{\mathbf{m}_M}\}$. Their mean converges to the numerator of Eq. (6),

$$\lim_{M\to\infty} \left\langle p^\sigma_{\mathbf{m}_{j=1}^M} \right\rangle_\rho := \lim_{M\to\infty} \frac{1}{M}\sum_{j=1}^{M} p^\sigma_{\mathbf{m}_j} = \sum_{\mathbf{m}} p^\rho_{\mathbf{m}} p^\sigma_{\mathbf{m}}. \quad (8)$$

The denominator of Eq. (6) can be estimated similarly with a separate classical simulation, by running the σ-circuit M' times, and computing the mean of probabilities $\{p^\sigma_{\mathbf{m}_j}\}$. This way we get

$$\lim_{M'\to\infty} \left\langle p^\sigma_{\mathbf{m}_{j=1}^{M'}} \right\rangle_\sigma := \lim_{M'\to\infty} \frac{1}{M'}\sum_{j=1}^{M'} p^\sigma_{\mathbf{m}_j} = \sum_{\mathbf{m}} \left(p^\sigma_{\mathbf{m}}\right)^2. \quad (9)$$

Both equations above are well-defined, and in this protocol each run of the circuit is used, so no postselection is required. This should lead to a general protocol for experimentally probe MIPTs, although a full classical simulation is still necessary, and the experimentally accessible system size will be limited by the power of classical simulation.

To obtain a scalable protocol, we focus on the case where σ is a stabilizer state, and the circuit bulk $C_{\mathbf{m}}$ is composed of stabilizer operations (Clifford gates and Pauli measurements) [43–45]. At this point we do not put constraint on ρ. In this special case, the denominator of Eq. (6) can be computed exactly in polynomial time, without doing any sampling as in Eq. (9) (see Appendix B for details). Thus, we may rewrite Eq. (6) as

$$\chi_C = \sum_{\mathbf{m}} p^\rho_{\mathbf{m}} \frac{p^\sigma_{\mathbf{m}}}{\sum_{\mathbf{m}} \left(p^\sigma_{\mathbf{m}}\right)^2}, \quad (10)$$

and in analogy with Eq. (8),

$$\chi_C = \lim_{M\to\infty} \left\langle \frac{p^\sigma_{\mathbf{m}_{j=1}^M}}{\sum_{\mathbf{m}} \left(p^\sigma_{\mathbf{m}}\right)^2} \right\rangle_\rho. \quad (11)$$

For each run of the ρ-circuit, we obtain the measurement record $\mathbf{m}_j$ and we can compute $\frac{p^\sigma_{\mathbf{m}_j}}{\sum_{\mathbf{m}} (p^\sigma_{\mathbf{m}})^2}$ in polynomial time, and take its mean over runs. Since the circuit is Clifford, the new "observable" $\frac{p^\sigma_{\mathbf{m}_j}}{\sum_{\mathbf{m}} (p^\sigma_{\mathbf{m}})^2}$ is either 0 or 1 for a given $\mathbf{m}$,[2] and this average converges quickly with increasing M. We also see that χ_C will be bounded between 0 and 1.

We now provide numerical methods and results for χ across the transition. We consider two types of choices for the state ρ, and take σ to be a stabilizer state in both cases.

B. Numerical methods and results

1. *Stabilizer state ρ versus stabilizer state σ*

We first take ρ to be a stabilizer state, while keeping σ another stabilizer state. As we explain in Appendix B, now χ_C in Eq. (10) admits a closed form expression that does not involve any summation over $\mathbf{m}$, see Eq. (B6). This allows an exact calculation of χ_C without the need of performing any sampling, at the cost of introducing N extra qubits that record the measurement history. These qubits are usually called "registers".

A further simplification occurs when ρ is obtainable from σ via erasure or dephasing channels, so that the N register qubits can also be dispensed with; see Eq. (B10). We will focus on this case below, where the numerical simulation is most scalable so that we can confidently extrapolate the results to more general choices of ρ.

In Fig. 2(a), we plot $\chi = \mathbb{E}_C \chi_C$ for $\rho = \frac{1}{2^L}\mathbb{1}$ and $\sigma = (|0\rangle\langle 0|)^{\otimes L}$, which satisfies the condition above. The data shows a clear "crossing" of χ near the transition, confirming our expectation that χ is an order parameter for the MIPT. Indeed, in the large L limit and for $p < p_c$, χ approaches unity, demonstrating that the distributions

[2] Recall that for Cliffford circuits a measurement either has a deterministic outcome, or has random outcomes ± 1 with equal probabilities 1/2 [45]. Let N_{rand} be the number of measurements (out of the total N) whose outcome is randomly ± 1. There are $2^{N_{\text{rand}}}$ possible trajectories in total, and they occur with equal probability $p^\sigma_{\mathbf{m}} = 2^{-N_{\text{rand}}}$.

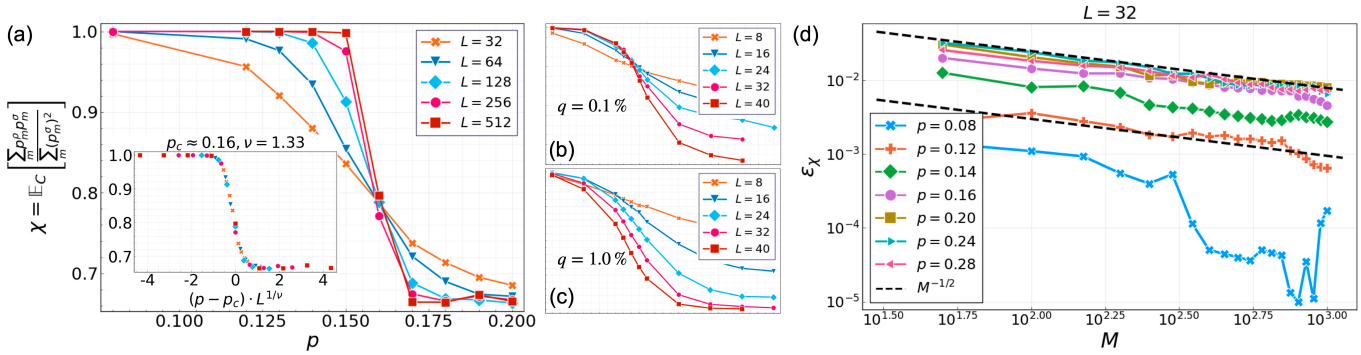

FIG. 2. (a) Numerical results for χ_C when averaged over 300 Clifford circuits in the bulk (denoted by $\mathbb{E}_C$), with the initial states $\rho = \frac{1}{2^L}\mathbb{1}$ and $\sigma = (|0\rangle\langle 0|)^{\otimes L}$. Here, for each C, the calculation is exact, and M can be thought of as infinity in Eq. (11). (Inset) Collapsing the data to a scaling form, with parameters p_c and ν close to those found near the MIPT in entanglement entropy [3, 9]. (b,c) The bahavior of χ when depolarizing noise is present in the ρ-circuit. As we see, at noise rate $q = 0.1\%$ (b), there is still evidence for a phase transition, although the location of the transition has shifted from $p_c \approx 0.16$ to $p_c \approx 0.14$. At noise rate 1% (c), there is no crossing, and any signature of the phase transition is completely washed out. (d) The fluctuation in χ from a finite number M of samples, as defined in Eq. (12).

of measurement outcomes become equal, independent of the initial state. Moreover, data collapse in Fig. 2(d) shows good agreement to a standard scaling form, with numerical values of the location of the transition p_c and of the critical exponent ν close to previous characterizations of the MIPT [9].

Although in the exact method for Fig. 2(a) no sampling of the measurement results is needed in the numerics (and we have essentially taken the limit $M \to \infty$ in Eq. (11)), we nevertheless simulate the sampling process for a finite M and compute the mean in Eq. (11). By comparing this to the exact result, we calculate the following measure of statistical fluctuations,

$$\varepsilon_\chi := \mathbb{E}_C\left[\left|\left\langle \frac{p^\sigma_{\mathbf{m}_{j=1}^M}}{\sum_{\mathbf{m}}(p^\sigma_{\mathbf{m}})^2}\right\rangle_\rho - \chi_C\right|\right]. \tag{12}$$

As we increase M we find $\varepsilon_\chi \propto M^{-1/2}$, as shown in Fig. 2(d). This is consistent with the samples $\left\{\frac{p^\sigma_{\mathbf{m}_{j=1}^M}}{\sum_{\mathbf{m}}(p^\sigma_{\mathbf{m}})^2}\right\}$ being bounded and having weak correlations.[3]

We also consider the effect of depolarizing noise, occuring randomly in the ρ-circuit with probability q per qubit per time step; whereas the σ-circuit is still taken to be noiseless. The setup is to mimic an experimental sampling procedure, where we run the ρ-circuit on a quantum processor subject to noise, whereas our supplementary classical simulation of the σ-circuit is noiseless. The depolarizing noise acts as a symmetry-breaking field in the effective spin model [6, 7, 30, 31, 46–48],[4] and in its presence the MIPT is no longer sharply defined. Nevertheless, evidence of the MIPT may still be observable if the error rate is small compared to the inverse spacetime volume of the circuit, as we see in Fig. 2(b,c).

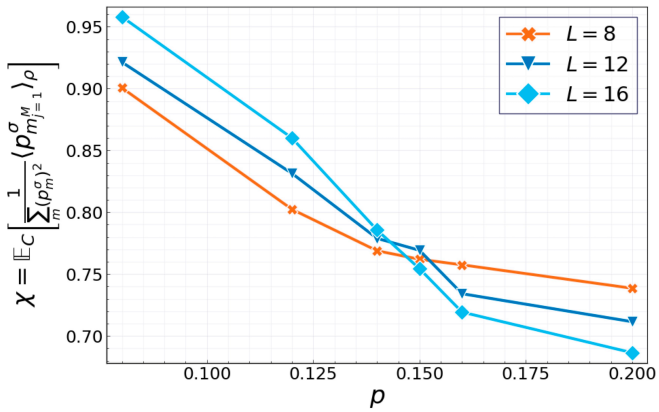

FIG. 3. Numerical results of χ for initial states $\rho = (|0\rangle\langle 0|)^{\otimes L/2} \otimes (|T\rangle\langle T|)^{\otimes L/2}$ (see Eq. (13)) and $\sigma = (|0\rangle\langle 0|)^{\otimes L}$, following the procedure in Eq. (11). Despite a different choice of initial state and smaller system sizes, the results are qualitatively similar to Fig. 2(a). Here the number of circuit realizations is 300, and for each circuit $M = 100$ shots of the circuit are taken.

2. *Magic state ρ versus stabilizer state σ*

We take ρ to be a non-stabilizer state, and σ to be a stabilizer state. In particular, we choose a state with $|0\rangle$

[3] Besides ε_χ, χ_C has additional fluctuations around the layout average χ due to difference choices of unitary gates which are suppressed for large space-time volume.

[4] See also Refs. [49–51] for related discusssion in random unitary circuits.

and $|T\rangle$ on alternating sites,

$$\rho = \bigotimes_{i=1}^{L/2} (|0\rangle\langle 0|_{2i-1} \otimes |T\rangle\langle T|_{2i}), \tag{13}$$

where $|T\rangle = \frac{1}{\sqrt{2}}\left(|0\rangle + e^{i\pi/4}|1\rangle\right)$ is a magic state. We still take the other initial state to be $\sigma = (|0\rangle\langle 0|)^{\otimes L}$.

Based on our calculation in Appendix A, we expect χ_C to exhibit similar behavior as in Sec. II B 1. This is confirmed in Fig. 3, where we follow the sampling procedure in Eq. (11). In particular, for a given C, we take $L \in \{8, 12, 16\}$, and sample $M = 100$ measurement trajectories, and compute $\left\langle \frac{p^\sigma_{\mathbf{m}M}}{\sum_{\mathbf{m}}(p^\sigma_{\mathbf{m}})^2} \right\rangle_\rho \approx \chi_C$. We then take the average over many different choices of C, namely $\mathbb{E}_C \left\langle \frac{p^\sigma_{\mathbf{m}M}}{\sum_{\mathbf{m}}(p^\sigma_{\mathbf{m}})^2} \right\rangle_\rho \approx \mathbb{E}_C \chi_C$. We observe a crossing of χ near $p \approx p_c \approx 0.16$.

It is important to notice that though the classical side of the computation (the σ-circuit) can be carried out efficiently, the quantum side (the ρ-circuit) is still classically hard [52]. This limits the system sizes that we can access classically in Fig. 3, but we hope larger system sizes can be achieved on near-term quantum processors.

C. Necessity of the encoding stage

Here we briefly discuss the choice of the circuit architecture in Fig. 1, in particular the inclusion of an encoding stage. In the usual setup [9] without the encoding stage, and when the two initial states differ on an extensive number of qubits, χ should vanish as $L \to \infty$ for all values of p, and thus cannot be used to probe the transition (see Appendix A 2). When ρ and σ differ only on a constant number of qubits χ would be instead related to a local spontaneous magnetization [7, 34], having the following scaling form near the transition,

$$\chi \approx \begin{cases} |p - p_c|^\beta + \chi_0, & p < p_c \\ \chi_0, & p > p_c \end{cases},$$

see Appendix A 2 for a detailed discussion. In this case, we do not expect a crossing as in Fig. 2, but instead a collapse of the curves for different system sizes L. In experiments, a collapse is likely harder to detect than a crossing. Moreover, the collapse will be more susceptible to noise for a given system size; that is, the collapse will immediately disappaear for any rate of noise. For this reason, we have chosen to focus on the circuit with an encoding stage throughout the paper.

Moreover, for the purpose of observing MIPT, including the encoding stage should only introduce minor experimental overhead. For example, noise in the encoding stage $t \in [0, t_{\text{encoding}}]$ would not affect the signal for MIPT in any important way as its effect can be accounted for by a different choice of ρ, which is not essential (see discussions in Appendix A); only noise in the circuit bulk $t \in [t_{\text{encoding}}, t_{\text{encoding}} + t_{\text{bulk}}]$ is important (see Fig. 2(b,c)).

III. DISCUSSIONS

Our protocol requires a simulation of many instances of the random hybrid circuit with mid-circuit measurements, and for each instance $O(1/\varepsilon^2)$ trajectories to estimate the cross-entropy to accuracy ε. This should be a task of similar complexity to Google's simulation of random unitary circuits [42], except that here we do not make measurements on the output state but in the bulk. However, different from that experiment, for observing the MIPT it suffices to focus on Clifford circuits, for which the classical simulation is not hard. This protocol is thus as scalable as the quantum processors. Our protocol does not require extra quantum operations, and is flexible in the choice of the initial state. The signal for the phase transition persists at $L = 40$ for sufficiently weak ($\approx 0.1\%$) depolarizing noise. Thus, we hope this protocol might be achievable on existing or near-term devices.

We emphasize that if the circuit is not composed of Clifford gates, our protocol is expected to require exponential classical resources. It is presently unclear whether it is in fact possible to probe the MIPT beyond Clifford circuits with polynomial resources [29].

Although the classical simulation is chosen to be easy for practical purposes, in our protocol the quantum simulation is classically hard for a generic choice of the initial state, which would result in a highly nontrivial output state. Our numerical results in Appendix C suggest that sampling measurement outcomes on the output state of the quantum simulation is classically hard in the volume law phase. Whether this can be used in practice for demonstrating quantum advantage is not known, due to apparent need of postselection in order to sample from this distribution.

Motivated by recent developments in benchmarking using random circuits [53–55], it is tempting to speculate that our protocol may be also useful in that context. Indeed, a successful observation of the MIPT would be a testament that the underlying device remains coherent until the very end. In particular, hybrid cricuits with mid-circuit measurements may be telling of the scaling of decoherence with respect to circuit depth. Such analyses may involve the behavior of entanglement in "shallow" hybrid circuits [46, 47].

Another interesting question is the (classical) sampling complexity of the bulk measurement outcomes in a hybrid Clifford circuit with magic initial states. We have shown that the bulk measurement history in the volume law phase does not depend on the initial state, and thus may be reproduced in polynomial time for a Clifford circuit with a stabilizer initial state. Similarly, in the area law phase and at the critical point, a classical simulation using matrix product states can (also) serve as a

polynomial-time sampler, due to low entanglement entropy. Thus, in one spatial dimension, sampling classically from the bulk measurement outcome distribution should, in principle, always be easy. The situation is much less clear in the area law phase of two dimensional hybrid circuits [22, 56].

ACKNOWLEDGEMENTS

We thank Jacob Hauser, Jin Ming Koh, Ali Lavasani, Austin Minnich, Mario Motta, Alan Morningstar, Xiao-Liang Qi, Shi-Ning Sun, Shengqi Sang, Jonathan Thio, Sagar Vijay, and Sisi Zhou for helpful discussions. YL is grateful for the hospitality of Vedika Khemani at Stanford University, where much of this work was undertaken. This work was supported by the Heising-Simons Foundation (YL and MPAF), and by the Simons Collaboration on Ultra-Quantum Matter, which is a grant from the Simons Foundation (651457, MPAF). Use was made of computational facilities purchased with funds from the National Science Foundation (CNS-1725797) and administered by the Center for Scientific Computing (CSC). The CSC is supported by the California NanoSystems Institute and the Materials Research Science and Engineering Center (MRSEC; NSF DMR-1720256) at UC Santa Barbara. YZ is supported by the Q-FARM fellowship at Stanford University. PG is supported by the Alfred P. Sloan Foundation through Grant FG-2020-13615, the Department of Energy through Award DE-SC0019380, and the Simons Foundation through Award No. 620869. EA is supported in part by the NSF QLCI program through grant number OMA-2016245.

[1] B. Skinner, J. Ruhman, and A. Nahum, Physical Review X **9**, 031009 (2019), arXiv:1808.05953 [cond-mat.stat-mech].
[2] A. Chan, R. M. Nandkishore, M. Pretko, and G. Smith, Phys. Rev. B **99**, 224307 (2019), arXiv:1808.05949 [cond-mat.stat-mech].
[3] Y. Li, X. Chen, and M. P. A. Fisher, Physical Review B **98**, 205136 (2018), arXiv:1808.06134 [quant-ph].
[4] S. Choi, Y. Bao, X.-L. Qi, and E. Altman, Phys. Rev. Lett. **125**, 030505 (2020), arXiv:1903.05124 [quant-ph].
[5] M. J. Gullans and D. A. Huse, Physical Review X **10**, 041020 (2020), arXiv:1905.05195 [quant-ph].
[6] C.-M. Jian, Y.-Z. You, R. Vasseur, and A. W. W. Ludwig, Phys. Rev. B **101**, 104302 (2020), arXiv:1908.08051 [cond-mat.stat-mech].
[7] Y. Bao, S. Choi, and E. Altman, Phys. Rev. B **101**, 104301 (2020), arXiv:1908.04305 [cond-mat.stat-mech].
[8] X. Cao, A. Tilloy, and A. De Luca, SciPost Physics **7**, 024 (2019), arXiv:1804.04638 [cond-mat.stat-mech].
[9] Y. Li, X. Chen, and M. P. A. Fisher, Physical Review B **100**, 134306 (2019), arXiv:1901.08092 [cond-mat.stat-mech].
[10] M. Szyniszewski, A. Romito, and H. Schomerus, Phys. Rev. B **100**, 064204 (2019), arXiv:1903.05452 [cond-mat.stat-mech].
[11] Q. Tang and W. Zhu, Physical Review Research **2**, 013022 (2020), arXiv:1908.11253 [cond-mat.stat-mech].
[12] A. Nahum and B. Skinner, Physical Review Research **2**, 023288 (2020), arXiv:1911.11169 [cond-mat.stat-mech].
[13] J. Lopez-Piqueres, B. Ware, and R. Vasseur, arXiv e-prints , arXiv:2003.01138 (2020), arXiv:2003.01138 [cond-mat.stat-mech].
[14] A. Lavasani, Y. Alavirad, and M. Barkeshli, Nature Physics **17**, 342 (2021), arXiv:2004.07243 [quant-ph].
[15] S. Sang and T. H. Hsieh, Physical Review Research **3**, 023200 (2021), arXiv:2004.09509 [cond-mat.stat-mech].
[16] M. Ippoliti, M. J. Gullans, S. Gopalakrishnan, D. A. Huse, and V. Khemani, Physical Review X **11**, 011030 (2021), arXiv:2004.09560 [quant-ph].
[17] X. Chen, Y. Li, M. P. A. Fisher, and A. Lucas, Physical Review Research **2**, 033017 (2020), arXiv:2004.09577 [quant-ph].
[18] Y. Fuji and Y. Ashida, arXiv e-prints , arXiv:2004.11957 (2020), arXiv:2004.11957 [cond-mat.stat-mech].
[19] O. Alberton, M. Buchhold, and S. Diehl, Phys. Rev. Lett. **126**, 170602 (2021), arXiv:2005.09722 [cond-mat.stat-mech].
[20] O. Lunt and A. Pal, arXiv e-prints , arXiv:2005.13603 (2020), arXiv:2005.13603 [quant-ph].
[21] S. Vijay, arXiv e-prints , arXiv:2005.03052 (2020), arXiv:2005.03052 [quant-ph].
[22] X. Turkeshi, R. Fazio, and M. Dalmonte, arXiv e-prints , 2007.02970 (2020), arXiv:2007.02970 [cond-mat.stat-mech].
[23] A. Nahum, S. Roy, B. Skinner, and J. Ruhman, arXiv e-prints , arXiv:2009.11311 (2020), arXiv:2009.11311 [cond-mat.stat-mech].
[24] Y. Bao, S. Choi, and E. Altman, arXiv e-prints , arXiv:2102.09164 (2021), arXiv:2102.09164 [cond-mat.stat-mech].
[25] U. Agrawal, A. Zabalo, K. Chen, J. H. Wilson, A. C. Potter, J. H. Pixley, S. Gopalakrishnan, and R. Vasseur, arXiv e-prints , arXiv:2107.10279 (2021), arXiv:2107.10279 [cond-mat.dis-nn].
[26] F. Barratt, U. Agrawal, S. Gopalakrishnan, D. A. Huse, R. Vasseur, and A. C. Potter, arXiv e-prints , arXiv:2111.09336 (2021), arXiv:2111.09336 [quant-ph].
[27] J. M. Koh, S.-N. Sun, M. Motta, and A. J. Minnich, (2022), arXiv:2203.04338 [quant-ph].
[28] C. Noel, P. Niroula, D. Zhu, A. Risinger, L. Egan, D. Biswas, M. Cetina, A. V. Gorshkov, M. J. Gullans, D. A. Huse, and C. Monroe, arXiv e-prints , arXiv:2106.05881 (2021), arXiv:2106.05881 [quant-ph].
[29] H. Dehghani, A. Lavasani, M. Hafezi, and M. J. Gullans, (2022), arXiv:2204.10904 [quant-ph].
[30] M. Ippoliti and V. Khemani, Phys. Rev. Lett. **126**, 060501 (2021), arXiv:2010.15840 [cond-mat.dis-nn].
[31] M. Ippoliti, T. Rakovszky, and V. Khemani, arXiv e-prints , arXiv:2103.06873 (2021), arXiv:2103.06873 [quant-ph].
[32] T.-C. Lu and T. Grover, arXiv e-prints , arXiv:2103.06356 (2021), arXiv:2103.06356 [quant-

ph].
[33] M. Buchhold, T. Müller, and S. Diehl, arXiv e-prints , arXiv:2208.10506 (2022), arXiv:2208.10506 [cond-mat.dis-nn].
[34] M. J. Gullans and D. A. Huse, Phys. Rev. Lett. **125**, 070606 (2020), arXiv:1910.00020 [cond-mat.stat-mech].
[35] A. Nahum, S. Vijay, and J. Haah, Physical Review X **8**, 021014 (2018), arXiv:1705.08975 [cond-mat.str-el].
[36] T. Zhou and A. Nahum, Phys. Rev. B **99**, 174205 (2019), arXiv:1804.09737 [cond-mat.stat-mech].
[37] R. Fan, S. Vijay, A. Vishwanath, and Y.-Z. You, Phys. Rev. B **103**, 174309 (2021), arXiv:2002.12385 [cond-mat.stat-mech].
[38] Y. Li and M. P. A. Fisher, Phys. Rev. B **103**, 104306 (2021), arXiv:2007.03822 [quant-ph].
[39] L. Fidkowski, J. Haah, and M. B. Hastings, Quantum **5**, 382 (2021), arXiv:2008.10611 [quant-ph].
[40] B. Yoshida, arXiv e-prints , arXiv:2109.08691 (2021), arXiv:2109.08691 [quant-ph].
[41] S. Boixo, S. V. Isakov, V. N. Smelyanskiy, R. Babbush, N. Ding, Z. Jiang, M. J. Bremner, J. M. Martinis, and H. Neven, arXiv e-prints , arXiv:1608.00263 (2016), arXiv:1608.00263 [quant-ph].
[42] F. Arute *et al.*, Nature **574**, 505 (2019), arXiv:1910.11333 [quant-ph].
[43] D. Gottesman, *Stabilizer codes and quantum error correction*, Ph.D. thesis, California Institute of Technology (1997), arXiv:quant-ph/9705052 [quant-ph].
[44] D. Gottesman, arXiv e-prints , quant-ph/9807006 (1998), arXiv:quant-ph/9807006 [quant-ph].
[45] S. Aaronson and D. Gottesman, Physical Review A **70**, 052328 (2004), arXiv:quant-ph/0406196 [quant-ph].
[46] Y. Li, X. Chen, A. W. W. Ludwig, and M. P. A. Fisher, arXiv e-prints , arXiv:2003.12721 (2020), arXiv:2003.12721 [quant-ph].
[47] Y. Li, S. Vijay, and M. P. A. Fisher, arXiv e-prints , arXiv:2105.13352 (2021), arXiv:2105.13352 [cond-mat.stat-mech].
[48] S.-K. Jian, C. Liu, X. Chen, B. Swingle, and P. Zhang, arXiv e-prints , arXiv:2106.09635 (2021), arXiv:2106.09635 [quant-ph].
[49] K. Noh, L. Jiang, and B. Fefferman, arXiv e-prints , arXiv:2003.13163 (2020), arXiv:2003.13163 [quant-ph].
[50] A. Deshpande, P. Niroula, O. Shtanko, A. V. Gorshkov, B. Fefferman, and M. J. Gullans, (2021), arXiv:2112.00716 [quant-ph].
[51] A. M. Dalzell, N. Hunter-Jones, and F. G. S. L. Brandão, (2021), arXiv:2111.14907 [quant-ph].
[52] S. Bravyi and D. Gosset, Phys. Rev. Lett. **116**, 250501 (2016), arXiv:1601.07601 [quant-ph].
[53] Y. Liu, M. Otten, R. Bassirianjahromi, L. Jiang, and B. Fefferman, arXiv e-prints , arXiv:2105.05232 (2021), arXiv:2105.05232 [quant-ph].
[54] D. K. Mark, J. Choi, A. L. Shaw, M. Endres, and S. Choi, arXiv e-prints , arXiv:2205.12211 (2022), arXiv:2205.12211 [quant-ph].
[55] J. R. Wootton, arXiv e-prints , arXiv:1806.02736 (2018), arXiv:1806.02736 [quant-ph].
[56] Q. Tang, X. Chen, and W. Zhu, Phys. Rev. B **103**, 174303 (2021), arXiv:2101.04320 [cond-mat.stat-mech].
[57] T. Zhou and A. Nahum, arXiv e-prints , arXiv:1912.12311 (2019), arXiv:1912.12311 [cond-mat.str-el].
[58] J. Cardy, arXiv e-prints , hep-th/0411189 (2004), arXiv:hep-th/0411189 [hep-th].
[59] I. Affleck and A. W. W. Ludwig, Phys. Rev. Lett. **67**, 161 (1991).
[60] S. Zhou, Z.-C. Yang, A. Hamma, and C. Chamon, SciPost Physics **9**, 087 (2020), arXiv:1906.01079 [cond-mat.stat-mech].
[61] J. Iaconis, arXiv e-prints , arXiv:2009.05512 (2020), arXiv:2009.05512 [quant-ph].

Appendix A: Cross entropy as boundary correlation function

1. Bulk cross entropy with encoding

We unpack the circuit averaged linear cross-entropy χ defined in Eq. (7),

$$\begin{aligned}\chi &:= \mathbb{E}_C \chi_C \\ &= \mathbb{E}_C \frac{\sum_{\mathbf{m}} p^{\rho}_{\mathbf{m}} p^{\sigma}_{\mathbf{m}}}{\sum_{\mathbf{m}} \left(p^{\sigma}_{\mathbf{m}}\right)^2} \\ &= \mathbb{E}_C \frac{\sum_{\mathbf{m}} \left(\operatorname{tr} C_{\mathbf{m}} \rho C^{\dagger}_{\mathbf{m}}\right) \left(\operatorname{tr} C_{\mathbf{m}} \sigma C^{\dagger}_{\mathbf{m}}\right)}{\sum_{\mathbf{m}} \left(\operatorname{tr} C_{\mathbf{m}} \sigma C^{\dagger}_{\mathbf{m}}\right)^2} \\ &= \mathbb{E}_C \frac{\sum_{\mathbf{m}} \operatorname{tr} C^{\otimes 2}_{\mathbf{m}} \cdot (\rho \otimes \sigma) \cdot C^{\dagger \otimes 2}_{\mathbf{m}}}{\sum_{\mathbf{m}} \operatorname{tr} C^{\otimes 2}_{\mathbf{m}} \cdot (\sigma \otimes \sigma) \cdot C^{\dagger \otimes 2}_{\mathbf{m}}}. \end{aligned} \tag{A1}$$

Recall that the letter C encodes the circuit layout (i.e. the locations of unitary gates and measurements) and the unitary gates, but not the measurement outcomes. The summation over $\mathbf{m}$ is taken inside the average, in both the numerator and denominator, independently. Thus, χ is different from the trajectory-averaged entanglement entropies that are used previously for identifying the MIPT. Nevertheless, in Fig. 2 we see that the location of the transition and the critical exponent ν do not change much when we use χ as an order parameter.

A proper treatment of the quenched average leads to a replicated spin model.[5] For our purposes here, we can instead consider the annealed average [37, 38], while keeping in mind that this is only a illustrative tool. In particular, consider

$$\overline{\chi} = \frac{\mathbb{E}_C \sum_{\mathbf{m}} \operatorname{tr} C^{\otimes 2}_{\mathbf{m}} \cdot (\rho \otimes \sigma) \cdot C^{\dagger \otimes 2}_{\mathbf{m}}}{\mathbb{E}_C \sum_{\mathbf{m}} \operatorname{tr} C^{\otimes 2}_{\mathbf{m}} \cdot (\sigma \otimes \sigma) \cdot C^{\dagger \otimes 2}_{\mathbf{m}}}. \tag{A2}$$

After the average over C, the numerator and the denominator each becomes an Ising partition function on a triangular lattice. They have bulk weights $J_p(s_i, s_j; s_k)$ for each downward-pointing triangle [6, 7] (see also Refs. [35, 36, 57]), and only differ in their boundary conditions. We denote them $Z_{\rho\sigma}$ and $Z_{\sigma\sigma}$, respectively.

We take ρ and σ to be products of local density matrices, i.e.

$$\rho = \prod_{x=1}^{L} \rho_x, \quad \sigma = \prod_{x=1}^{L} \sigma_x, \text{ where } \operatorname{tr} \rho_x = \operatorname{tr} \sigma_x = 1 \ \forall x. \tag{A3}$$

Moreover, we also have $\operatorname{tr} \sigma_x^2 = 1$ since we assumed σ is a pure product state. Thus,

$$\begin{aligned} Z_{\sigma\sigma} &= \sum_{\{s_i = \pm 1\}} \prod_{\langle i,j,k \rangle \in \nabla} J_p(s_i, s_j; s_k) \cdot \prod_{x \in \partial \mathcal{M}_T} \delta_{s_x = +1} \cdot \prod_{x \in \partial \mathcal{M}_0} \left(\delta_{s_x=+1} (\operatorname{tr} \sigma_x)^2 + \delta_{s_x=-1} \operatorname{tr}\left(\sigma_x^2\right)\right) \\ &= \sum_{\{s_i = \pm 1\}} \prod_{\langle i,j,k \rangle \in \nabla} J_p(s_i, s_j; s_k) \cdot \prod_{x \in \partial \mathcal{M}_T} \delta_{s_x = +1}, \end{aligned} \tag{A4}$$

and

$$\begin{aligned} Z_{\rho\sigma} &= \sum_{\{s_i = \pm 1\}} \prod_{\langle i,j,k \rangle \in \nabla} J_p(s_i, s_j; s_k) \cdot \prod_{x \in \partial \mathcal{M}_T} \delta_{s_x = +1} \cdot \prod_{x \in \partial \mathcal{M}_0} \left(\delta_{s_x=+1} (\operatorname{tr} \rho_x)(\operatorname{tr} \sigma_x) + \delta_{s_x=-1} \operatorname{tr}(\rho_x \cdot \sigma_x)\right) \\ &= \sum_{\{s_i = \pm 1\}} \prod_{\langle i,j,k \rangle \in \nabla} J_p(s_i, s_j; s_k) \cdot \prod_{x \in \partial \mathcal{M}_T} \delta_{s_x = +1} \cdot \prod_{x \in \partial \mathcal{M}_0} \left(\delta_{s_x=+1} + \delta_{s_x=-1} \operatorname{tr}(\rho_x \cdot \sigma_x)\right) \\ &= \sum_{\{s_i = \pm 1\}} \prod_{\langle i,j,k \rangle \in \nabla} J_p(s_i, s_j; s_k) \cdot \prod_{x \in \partial \mathcal{M}_T} \delta_{s_x = +1} \cdot \prod_{x \in \partial \mathcal{M}_0} e^{h_x (s_x - 1)}. \end{aligned} \tag{A5}$$

Here, we use $\partial \mathcal{M}_0$ to denote the $t = 0$ boundary of the circuit, and $\partial \mathcal{M}_T$ to denote the final time ($t = T$) boundary. We see that at $t = 0$, $Z_{\sigma\sigma}$ has a "free" boundary condition, and $Z_{\rho\sigma}$ has a magnetic field with strength $h_x = -\frac{1}{2} \ln [\operatorname{tr}(\rho_x \cdot \sigma_x)]$. At $t = T$, in both partition functions spins are fixed to be $s_x = +1$.

Our circuit in Fig. 1 has an "encoding" stage without measurements ($p = 0$) up until $t_{\text{encoding}} = 2L$. This makes the lower half of the circuit a pure unitary one, where domain walls with both endpoints on the $t = 0$ boundary are disallowed by the microscopics of the stat mech model [35, 36]. In this case, the finite-strength field at the $t = 0$ boundary of $Z_{\rho\sigma}$ becomes essentially infinite,

[5] Due to the difference we stressed above, this leads to a stat mech model that differs from those obtained in Refs. [6, 7]. In particular, the spins here take values in the permutation group $S_{Q=2n}$ with the replica limit $n \to 0$, and which has a different symmetry.

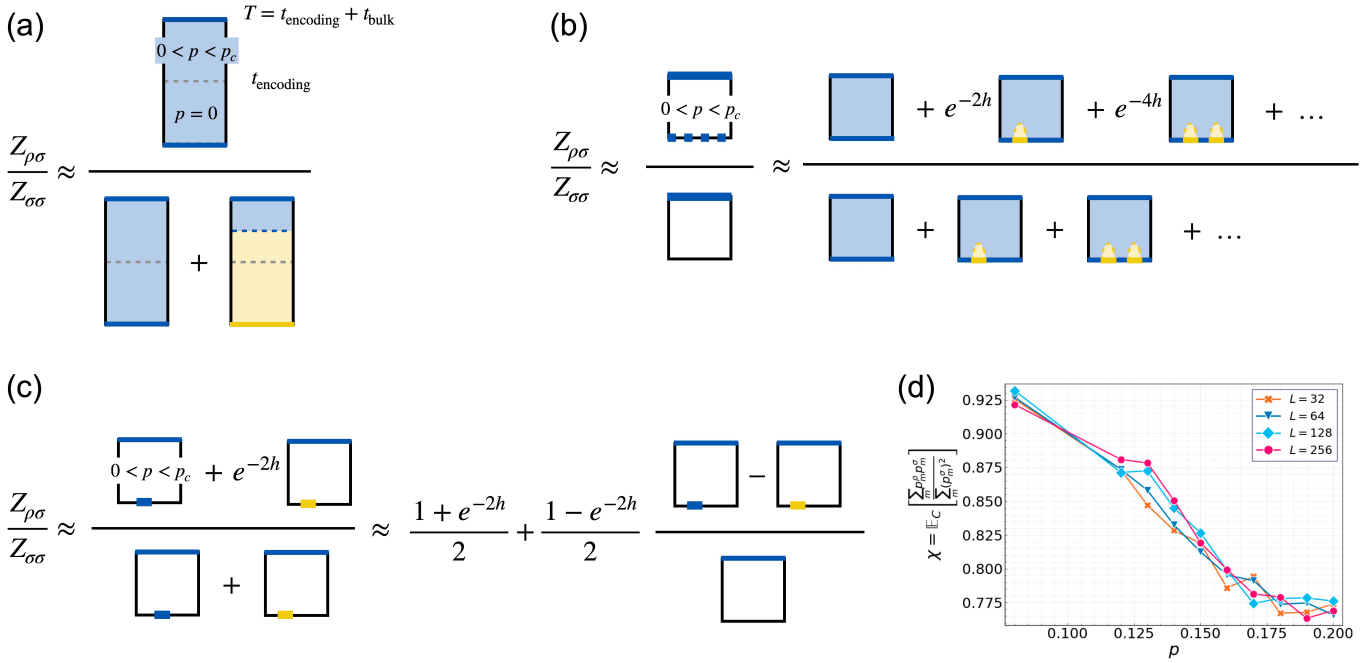

FIG. 4. (a) Pictorial representation of the partition function ratio $Z_{\rho\sigma}/Z_{\sigma\sigma}$ in Eq. (A8), for $p = 0$ in the encoding stage and $p < p_c$ in the circuit bulk. (b) Pictorial representation of the partition function ratio in Eq. (A10). Here we do not have an encoding stage, and there is a *uniform*, finite magnetic field of strength h (represented with a dashed line) applied at the $t = 0$ boundary. (c) Pictorial representation of the partition function ratio in Eq. (A11). Here we do not have an encoding stage, and there is a *local*, finite magnetic field of strength h applied at the $t = 0$ boundary. In this case, the cross entropy is expected to be a function p but not of L (see Eq. (A12)), as we confirm in (d). In all figures the blue color represents spins pointing in the "+" direction, the yellow color represents spins pointing in the "−" direction, and the black color represents a "free" boundary condition, where the spins can point in either direction.

putting a hard boundary condition at $t = 0$:

$$\begin{aligned} Z_{\rho\sigma} &\approx \sum_{\{s_i=\pm1\}} \prod_{\langle i,j,k\rangle\in\nabla} J_p(s_i, s_j; s_k) \\ &\quad \cdot \prod_{x\in\partial\mathcal{M}_T} \delta_{s_x=+1} \cdot \prod_{x\in\partial\mathcal{M}_0} \delta_{s_x=+1} \\ &:= Z_{++}, \end{aligned} \tag{A6}$$

where Z_{++} denotes the partition function with + boundary condition at $t = 0$ and + boundary condition at $t = T$. By the same reasonining and the same notation, we can rewrite

$$Z_{\sigma\sigma} \approx Z_{++} + Z_{-+}. \tag{A7}$$

We represent these partition functions diagrammatically in Fig. 4, where the boundary conditions are highlighted with color: blue for + and orange for −. (In the figure, we only illustrated the case where $p < p_c$ after the initial encoding stage; these two stages are separated by a gray, dashed line.) We have

$$\overline{\chi} = \frac{Z_{\rho\sigma}}{Z_{\sigma\sigma}} = \frac{1}{1 + Z_{-+}/Z_{++}}. \tag{A8}$$

In the volume law phase, we expect $Z_{-+}/Z_{++} \propto \exp(-O(L))$, because a domain wall with finite line tension of length L must be inserted between $t \in [t_{\text{encoding}}, T]$, to accommodate the boundary conditions change from − to + in time; see Fig. 4. On the other hand, in the area law phase, the domain wall line tension vanishes, and we have $Z_{-+}/Z_{++} = O(1)$. Thus,

$$\overline{\chi} = \begin{cases} 1 + \exp(-O(L)), & p < p_c \\ O(1), & p > p_c \end{cases}. \tag{A9}$$

Despite the fact that we are adopting an annealed average in $\overline{\chi}$, it captures the qualitative behavior of the quenched average χ in Sec. II in the two phases (but presumably not the critical properties).

2. Bulk cross entropy without encoding

Here we extend our discussion in Sec. II C on χ in the absence of the encoding stage, so that the entire two-dimensional magnet is now at finite temperature; see Fig. 4(b). Here, the partition functions $Z_{\sigma\sigma}$ and $Z_{\rho\sigma}$ have boundary conditions that are identical to those in Eqs. (A4, A5). However, the spins at the $t = 0$ boundary now need not be completely aligned, and small domain walls can be created at the cost of a finite free energy per unit length.

Using the same graphical notation as in Fig. 4(a), with an additional color, black, representing the "free" boundary condition f, and dashed blue line representing the finite strength boundary magnetic field h_x in the "+" direction at $t = 0$, we represent $\overline{\chi} = \frac{Z_{\rho\sigma}}{Z_{\sigma\sigma}}$ again with partition functions of appropriate boundary conditions in Fig. 4(b). First consider a case where the boundary magnetic field $h_x = -\frac{1}{2}\ln[\mathrm{tr}(\rho_x \cdot \sigma_x)]$ is uniform and independent of x. This would be the case when, say, $\rho = \frac{1}{2^L}\mathbb{1}$ and $\sigma = (|0\rangle\langle 0|)^{\otimes L}$. Let the free energy cost of a domain wall with unit length be δF and define the fugacity to be $y = e^{-\delta F}$, we have (compare Fig. 4(b))

$$\begin{aligned}\overline{\chi} &= \frac{Z_{\rho\sigma}}{Z_{\sigma\sigma}} \\ &= \frac{1 + \binom{L}{1}e^{-2h}y + \binom{L}{2}e^{-4h}y^2 + \dots}{1 + \binom{L}{1}y + \binom{L}{2}y^2 + \dots} \\ &\approx \frac{(1+e^{-2h}y)^L}{(1+y)^L}. \end{aligned} \tag{A10}$$

Both $Z_{\rho\sigma}$ and $Z_{\sigma\sigma}$ numerator are now a series of terms, with the i-th leading term having i domain walls each of unit length (neglecting their interactions). Thus, $\overline{\chi}$ is exponentially suppressed by L for any $h > 0$, thus negligible throughout the phase diagram.

We can also generalize Eq. (A10) to the case where ρ and σ only differ on one site, as discussed in Sec. II C. The partition functions are shown in Fig. 4(c), where we obtain

$$\overline{\chi} \approx \frac{1+e^{-2h}}{2} + \frac{1-e^{-2h}}{2}\langle s_{x\in\partial\mathcal{M}_0}\rangle_{s_{x\in\partial\mathcal{M}_T}=+1}. \tag{A11}$$

Here $\langle s_{x\in\partial\mathcal{M}_0}\rangle_{s_{x\in\partial\mathcal{M}_T}=+1}$ is the expectation value of a boundary spin. Thus, we expect the following behavior of χ near the critical point:

$$\overline{\chi} \approx \begin{cases} |p-p_c|^\beta + \chi_0, & p < p_c \\ \chi_0, & p > p_c \end{cases}. \tag{A12}$$

Here, $\chi_0 \approx \frac{1+e^{-2h}}{2}$ is a nonuniversal constant between 0 and 1. This expectation is confirmed by numerical results in Fig. 4(d).

3. Higher order cross entropies and the Kullback-Leibler divergence

Here we compute another measure of the difference between the two probability distributions $p^\rho_{\mathbf{m}}$ and $p^\sigma_{\mathbf{m}}$, the Kullback-Leibler divergence,

$$D_{\mathrm{KL}}(p^\rho|p^\sigma) = \sum_{\mathbf{m}}(p^\rho_{\mathbf{m}}\log p^\rho_{\mathbf{m}} - p^\rho_{\mathbf{m}}\log p^\sigma_{\mathbf{m}}). \tag{A13}$$

This can be computed by the replica trick, where we introduce an integer replica index Q and the higher-order cross entropies

$$\chi_Q = \mathbb{E}_C \frac{\sum_{\mathbf{m}} p^\rho_{\mathbf{m}}(p^\sigma_{\mathbf{m}})^{Q-1}}{\sum_{\mathbf{m}}(p^\rho_{\mathbf{m}})^Q}. \tag{A14}$$

When $Q = 2$, this reduces to the linear cross entropy Eq. (6) with the roles of ρ and σ exchanged. Thus, this quantity cannot be sampled using the method presented in the main text.

In order to understand the higher-order cross entropies in terms of the stat-mech model, we again resort to the annealed average

$$\overline{\chi}_Q = \frac{\mathbb{E}_C \sum_{\mathbf{m}} p^\rho_{\mathbf{m}}(p^\sigma_{\mathbf{m}})^{Q-1}}{\mathbb{E}_C \sum_{\mathbf{m}}(p^\rho_{\mathbf{m}})^Q} \tag{A15}$$

Although the two quantities χ_Q and $\overline{\chi}_Q$ are different in general, they become the same quantity in the limit $Q \to 1$. More precisely, at $Q = 1$, $\chi_Q = \overline{\chi}_Q = 1$ and

$$\left.\frac{d\chi_Q}{dQ}\right|_{Q=1} = \left.\frac{d\overline{\chi}_Q}{dQ}\right|_{Q=1} = -\mathbb{E}_C D_{\mathrm{KL}}(p^\rho|p^\sigma). \tag{A16}$$

In order to see this, we expand Eq. (A14) to first order in $Q-1$,

$$\begin{aligned}\chi_Q &= \mathbb{E}_C \frac{1 + (Q-1)\sum_{\mathbf{m}} p^\rho_{\mathbf{m}}\log p^\sigma_{\mathbf{m}} + O((Q-1)^2)}{1 + (Q-1)\sum_{\mathbf{m}} p^\rho_{\mathbf{m}}\log p^\rho_{\mathbf{m}} + O((Q-1)^2)} \\ &= 1 + (Q-1)\mathbb{E}_C\sum_{\mathbf{m}}(p^\rho_{\mathbf{m}}\log p^\sigma_{\mathbf{m}} - p^\rho_{\mathbf{m}}\log p^\rho_{\mathbf{m}}) + O((Q-1))^2 \\ &= 1 - (Q-1)\mathbb{E}_C D_{\mathrm{KL}}(p^\rho|p^\sigma) + O((Q-1)^2), \end{aligned} \tag{A17}$$

Expanding Eq. (A15) to the first order, we obtain the same expression.

Next, we compute $\overline{\chi}_Q$ using the stat mech model assuming Haar random gates in the circuit. Notice that this quantity can be infinite in general for Clifford circuits. The spins on the honeycomb lattice take on $Q!$ different values labelled by group elements of S_Q, with three-body ferromagnetic interactions on each downward-pointing

triangles [6, 7]. The model has an $S_Q \times S_Q$ symmetry, which is spontaneously broken in the volume law phase. Assuming Eq. (A3), and repeating the derivation on the boundary conditions that leads to Eq. (A8), we obtain

$$\overline{\chi}_Q = \frac{Z_{Q,\rho\sigma}}{Z_{Q,\rho\rho}}, \tag{A18}$$

where

$$Z_{Q,\rho\sigma} = \sum_{g\in S_{Q-1}} Z_{Q,ge} \tag{A19}$$

$$Z_{Q,\rho\rho} = \sum_{g\in S_Q} Z_{Q,ge}, \tag{A20}$$

and $Z_{Q,ge}$ is the partition function of the spin model with fixed boundary condition $g \in S_Q$ on the bottom boundary and fixed boundary condition e (identity permutation) on the top boundary, S_{Q-1} is the subgroup of S_Q of permutations that keeps the first element invariant. In the volume law phase ($p < p_c$), domain walls have finite tension, thus $Z_{Q,ge}/Z_{Q,ee} = O(e^{-L})$ for every $g \neq e$. As a result $Z_{Q,\rho\sigma} \approx Z_{Q,\rho\rho} \approx Z_{Q,ee}$ and $\bar{\chi}_Q = 1 + O(e^{-L})$. In the area law phase the partition functions with different boundary conditions are on the same order and $\bar{\chi}_Q$ is an order one number that depends on Q. These results are completely analogous with the case of $Q = 2$ as they involve similar arguments.

At the critical point ($p = p_c$), assuming periodic boundary conditions in the spatial direction, Z_{ge} is a partition function of the CFT on a finite cylinder with width L and length T. The partition function can be written in two equivalent forms [58]

$$Z_{Q,ge} = \sum_\alpha \langle\alpha|g\rangle\langle e|\alpha\rangle e^{-2\pi(\Delta_{Q,\alpha} - c_Q/12)T/L} \tag{A21}$$

$$= \sum_\beta N_\beta^{ge} e^{-\pi(h_{Q,\beta} - c_Q/24)L/T}. \tag{A22}$$

In the first expression, α runs over *bulk* operators, $|g\rangle$ and $\langle e|$ are Cardy states corresponding to the two fixed boundary conditions, $\Delta_{Q,\alpha}$ is the bulk scaling dimension, c_Q is the central charge. In the second expression, β runs over *boundary* operators, $h_{Q,\beta}$ is the scaling dimension of the boundary operator, N_β^{ge} is the multiplicity of the boundary condition changing operator from boundary condition g to boundary condition e. The first expression is useful when $T \gg L$, then we only keep the ground state $\alpha = \mathbb{1}$ in the sum. The second expression is useful when $T \ll L$, then we only keep the leading boundary condition changing operator in the sum. Thus,

$$Z_{Q,ge} = \begin{cases} e^{s_{Q,e}+s_{Q,g}} e^{-\pi c_Q T/(6L)} & (T \gg L) \\ e^{-\pi(h_{Q,ge} - c_Q/24)L/T} & (T \ll L) \end{cases}, \tag{A23}$$

where $s_{Q,g} \equiv \log(\langle\mathbb{1}|g\rangle)$ is known as the Affleck-Ludwig boundary entropy [59], $h_{Q,ge}$ is the scaling dimension of the lowest boundary condition changing operator from g to e. Thus, at replica index $Q \geq 2$, we obtain

$$\overline{\chi}_Q = \frac{\sum_{g\in S_{Q-1}} e^{s_{Q,g}}}{\sum_{g\in S_Q} e^{s_{Q,g}}} \quad (T \gg L) \tag{A24}$$

and

$$\overline{\chi}_Q = \frac{\sum_{g\in S_{Q-1}} e^{-\pi h_{Q,ge} L/T}}{\sum_{g\in S_Q} e^{-\pi h_{Q,ge} L/T}} \quad (T \ll L) \tag{A25}$$

We focus on the long time limit $T \gg L$, starting with Eq. (A24). Since we are looking at the critical point, the symmetry is not spontaneously broken, and the ground state $|\mathbb{1}\rangle$ is invariant under the action of S_Q. Thus, $s_{Q,g}$ for all fixed boundary conditions g are the same, and we have

$$\overline{\chi}_Q = \frac{1}{Q} \quad (T \gg L) \tag{A26}$$

The situation is similar in the area law phase $p > p_c$, where an expansion similar to Eq. (A21) can be written down from the transfer matrix of the spin model. The spectrum here will become gapped, but in this limit only the ground state contributes. Moreover, the ground state still preserves the symmetry of the model. Summaring, we have

$$\overline{\chi}_Q = \begin{cases} 1, & T \gg L, p < p_c \\ 1/Q, & T \gg L, p \geq p_c \end{cases}, \tag{A27}$$

neglecting terms that are exponentially small in L. Taking the $Q \to 1$ limit we obtain

$$\mathbb{E}_C D_{\mathrm{KL}}(p^\rho|p^\sigma) = \begin{cases} 0, & T \gg L, p < p_c \\ 1, & T \gg L, p \geq p_c \end{cases}. \tag{A28}$$

Another closely related quantity is

$$\chi'_Q = \mathbb{E}_C \frac{\sum_{\mathbf{m}} p^\rho_{\mathbf{m}} (p^\sigma_{\mathbf{m}})^{Q-1}}{\sum_{\mathbf{m}} (p^\sigma_{\mathbf{m}})^Q}. \tag{A29}$$

This is reduced to Eq. (6) when $Q = 2$. For generic integer $Q \geq 2$, it can be sampled efficiently using the hybrid quantum-classical algorithm in the main text,

$$\chi'_Q = \left\langle \frac{(p^\sigma_{\mathbf{m}})^{Q-1}}{\sum_{\mathbf{m}} (p^\sigma_{\mathbf{m}})^Q} \right\rangle_\rho. \tag{A30}$$

As in $Q = 2$, it is expected that the sampling error decays as $M^{-1/2}$, where M is the sample size, since we are averging over random numbers with $O(1)$ amplitude. In order to interpret this quantity in the stat mech model, we consider the annealed average

$$\overline{\chi'_Q} = \frac{\mathbb{E}_C \sum_{\mathbf{m}} p^\rho_{\mathbf{m}} (p^\sigma_{\mathbf{m}})^{Q-1}}{\mathbb{E}_C \sum_{\mathbf{m}} (p^\sigma_{\mathbf{m}})^Q}. \tag{A31}$$

The quenched and annealed averages again coincide in the replica limit,

$$\frac{d\chi'}{dQ} = \frac{d\bar{\chi}'}{dQ} = \mathbb{E}_C \sum_{\mathbf{m}} (p^{\rho}_{\mathbf{m}} - p^{\sigma}_{\mathbf{m}}) \log p^{\sigma}_{\mathbf{m}}. \tag{A32}$$

This also measures the difference between the two probablity distributions, although it is not the KL divergence anymore. As long as ρ and σ are pure product states that are not identical, Eq. (A31) and Eq. (A15) are mapped to the same quantity in terms of the stat mech model. The argument that leads to Eq. (A34) goes through, and we obtain

$$\bar{\chi}'_Q = \begin{cases} 1, & T \gg L, p < p_c \\ 1/Q, & T \gg L, p \geq p_c \end{cases}, \tag{A33}$$

neglecting terms that are exponentially small in L. Taking the $Q \to 1$ limit we obtain

$$\mathbb{E}_C \sum_{\mathbf{m}} (p^{\sigma}_{\mathbf{m}} - p^{\rho}_{\mathbf{m}}) \log p^{\sigma}_{\mathbf{m}} = \begin{cases} 0, & T \gg L, p < p_c \\ 1, & T \gg L, p \geq p_c \end{cases}. \tag{A34}$$

4. Linear cross entropy with ancilla

In this Appendix we investigate how coupling to an ancilla may affect the signature of the transition. Suppose we extend the system, S, with a system of ancilla qudits W, so that the initial state is ρ_{SW} or σ_{SW}. In particular, we take $|W| = |S| = L$, and associate one ancilla qudit to each system qudit, collectively denoted as SW, x on site x. The evolution acts on system S as before, while the ancillae W are idlers, i.e. no evolution occurs. We denote the unnormalized output state when reduced to W by $\rho_{\mathbf{m}W} = \mathrm{tr}_S(C_{\mathbf{m}} \rho_{SW} C^{\dagger}_{\mathbf{m}})$, and we similarly define $\sigma_{\mathbf{m}W}$. We consider the quantity

$$\chi' = \frac{\sum_{\mathbf{m}} \mathrm{tr}_W \, \rho_{\mathbf{m}W} \sigma_{\mathbf{m}W}}{\sum_{\mathbf{m}} \mathrm{tr}_W \, \sigma^2_{\mathbf{m}W}} \tag{A35}$$

Differently from Eq. (6), which is a cross entropy between classical probability distributions, here χ' is a "quantum" cross entropy.

We shall consider two particular ways of coupling system and ancilla —one quantum and one classical. Each way of coupling will lead to a particular dependence of χ' on p which in turn may be used to diagnose the transition. We will always take initial product states $\rho_{SW} = \prod_x \rho_{SW,x}$ and $\sigma_{SW} = \prod_x \sigma_{SW,x}$; moreover, for simplicity we shall asssume that the ancilla is decoupled from the system in the ρ state $\rho_{SW} = \rho_S \otimes \rho_W$. We will study two forms of σ_{SW}: 1) EPR state for the ancilla-system on each site each site x, $\sigma_{SW,x} = |I_x\rangle\langle I_x|$ with $|I_x\rangle = \frac{1}{\sqrt{d}} \sum_i |i_{S,x} i_{W,x}\rangle$, and 2) classically correlated state $\sigma_{SW,x} = \frac{1}{d} \sum_i |i_{S,x} i_{W,x}\rangle\langle i_{S,x} i_{W,x}|$.

In the EPR pair case, we have (suppressing the x-dependence $\rho_{SW,x} \to \rho_{SW}$ and $\sigma_{SW,x} \to \sigma_{SW}$)

$$\begin{aligned} Z_{\rho\sigma} &= \sum_{\{s_i = \pm 1\}} \prod_{\langle i,j,k\rangle \in \nabla} J_p(s_i, s_j; s_k) \cdot \prod_{x \in \partial \mathcal{M}_T} \delta_{s_x = +1} \cdot \prod_{x \in \partial \mathcal{M}_0} \mathrm{tr}_W \left(\delta_{s_x=+1} (\mathrm{tr}_S \, \rho_{SW})(\mathrm{tr}_S \, \sigma_{SW}) + \delta_{s_x=-1} \, \mathrm{tr}_S(\rho_{SW} \cdot \sigma_{SW}) \right) \\ &= \sum_{\{s_i = \pm 1\}} \prod_{\langle i,j,k\rangle \in \nabla} J_p(s_i, s_j; s_k) \cdot \prod_{x \in \partial \mathcal{M}_T} \delta_{s_x = +1} \cdot \prod_{x \in \partial \mathcal{M}_0} \left(\delta_{s_x=+1} \cdot \frac{1}{d} + \delta_{s_x=-1} \cdot \frac{1}{d} \mathrm{tr}(\rho_S \rho_W) \right) = d^{-L} Z_{++} \end{aligned} \tag{A36}$$

$$\begin{aligned} Z_{\sigma\sigma} &= \sum_{\{s_i = \pm 1\}} \prod_{\langle i,j,k\rangle \in \nabla} J_p(s_i, s_j; s_k) \cdot \prod_{x \in \partial \mathcal{M}_T} \delta_{s_x = +1} \cdot \prod_{x \in \partial \mathcal{M}_0} \mathrm{tr}_W \left(\delta_{s_x=+1} (\mathrm{tr}_S \, \sigma_{SW})(\mathrm{tr}_S \, \sigma_{SW}) + \delta_{s_x=-1} \, \mathrm{tr}_S(\sigma_{SW} \cdot \sigma_{SW}) \right) \\ &= \sum_{\{s_i = \pm 1\}} \prod_{\langle i,j,k\rangle \in \nabla} J_p(s_i, s_j; s_k) \cdot \prod_{x \in \partial \mathcal{M}_T} \delta_{s_x = +1} \cdot \prod_{x \in \partial \mathcal{M}_0} \left(\delta_{s_x=+1} \cdot \frac{1}{d} + \delta_{s_x=-1} \right) = d^{-L} Z_{++} + Z_{-+} \,. \end{aligned} \tag{A37}$$

Where in the last step of each of the above equations we assumed $\mathrm{tr}(\rho_S \rho_W) < 1$. We see that

$$\bar{\chi} = \frac{Z_{\rho\sigma}}{Z_{\sigma\sigma}} = \frac{Z_{++}}{Z_{++} + d^L Z_{-+}} \,. \tag{A38}$$

The tension of domain walls in the Ising model (see Eq. (4)) decreases as p becomes finite, therefore $Z_{-+} \sim e^{-aL \log d}$ with $a < 1$. Therefore, as soon as $p > 0$, $\bar{\chi}$ becomes exponentially suppressed in system size L thus destroying the signature of the transition. This is because at the final time we have access to sufficient information about the initial quantum state of the system due to the highly-entangled ancilla-system coupling.

For the classically correlated state $\sigma_{SW} = \frac{1}{d} \sum_i |i_S i_W\rangle\langle i_S i_W|$, we have

$$Z_{\rho\sigma} = \sum_{\{s_i=\pm1\}} \prod_{\langle i,j,k\rangle\in\nabla} J_p(s_i,s_j;s_k)\cdot \prod_{x\in\partial\mathcal{M}_T}\delta_{s_x=+1}\cdot \prod_{x\in\partial\mathcal{M}_0} \mathrm{tr}_W\left(\delta_{s_x=+1}(\mathrm{tr}_S\,\rho_{SW})(\mathrm{tr}_S\,\sigma_{SW})+\delta_{s_x=-1}\,\mathrm{tr}_S(\rho_{SW}\cdot\sigma_{SW})\right)$$

$$= \sum_{\{s_i=\pm1\}} \prod_{\langle i,j,k\rangle\in\nabla} J_p(s_i,s_j;s_k)\cdot \prod_{x\in\partial\mathcal{M}_T}\delta_{s_x=+1}\cdot \prod_{x\in\partial\mathcal{M}_0}\left(\delta_{s_x=+1}\cdot\frac{1}{d}+\delta_{s_x=-1}\cdot\frac{1}{d}\,\mathrm{tr}(\tilde\rho_S\tilde\rho_W)\right) = d^{-L}Z_{++} \quad \text{(A39)}$$

$$Z_{\sigma\sigma} = \sum_{\{s_i=\pm1\}} \prod_{\langle i,j,k\rangle\in\nabla} J_p(s_i,s_j;s_k)\cdot \prod_{x\in\partial\mathcal{M}_T}\delta_{s_x=+1}\cdot \prod_{x\in\partial\mathcal{M}_0} \mathrm{tr}_W\left(\delta_{s_x=+1}(\mathrm{tr}_S\,\sigma_{SW})(\mathrm{tr}_S\,\sigma_{SW})+\delta_{s_x=-1}\,\mathrm{tr}_S(\sigma_{SW}\cdot\sigma_{SW})\right)$$

$$= \sum_{\{s_i=\pm1\}} \prod_{\langle i,j,k\rangle\in\nabla} J_p(s_i,s_j;s_k)\cdot \prod_{x\in\partial\mathcal{M}_T}\delta_{s_x=+1}\cdot \prod_{x\in\partial\mathcal{M}_0}\left(\delta_{s_x=+1}\cdot\frac{1}{d}+\delta_{s_x=-1}\cdot\frac{1}{d}\right) = d^{-L}Z_{++}+d^{-L}Z_{-+}\,, \quad \text{(A40)}$$

where $\tilde\rho=\sum_i\langle i|\rho|i\rangle|i\rangle\langle i|$ denotes a dephased state, and we assumed $\mathrm{tr}(\tilde\rho_S\tilde\rho_W)<1$. We now have

$$\bar\chi = \frac{Z_{\rho\sigma}}{Z_{\sigma\sigma}} = \frac{Z_{++}}{Z_{++}+Z_{-+}} \quad \text{(A41)}$$

and we find the same behavior as in the case without ancilla. We conclude that a classically correlated ancilla does not seem to qualitatively alter the signature of the transition. This is expected, as at the final time we only have access to classical information about the initial state.

Appendix B: Numerical algorithm for χ_C in Clifford circuits

We first recall a "purified" representation of the hybrid circuit. As pointed out in Refs. [5, 7], the dynamics of the hybrid circuit can be purified by introducing one "register" qubit for each single site measurement. In particular, each measurement can be replaced by a controlled-NOT (CNOT) gate from the measured qubit to the register, followed by a dephasing channel on the register.[6] With these, at the end of the time evolution we have the following joint state on physical qubits Q and register qubits R,

$$\rho_{QR} = \sum_{\mathbf{m}} C_{\mathbf{m}}\rho C_{\mathbf{m}}^\dagger\otimes|\mathbf{m}\rangle\langle\mathbf{m}|_R\,. \quad \text{(B4)}$$

And similarly for the initial state σ,

$$\sigma_{QR} = \sum_{\mathbf{m}} C_{\mathbf{m}}\sigma C_{\mathbf{m}}^\dagger\otimes|\mathbf{m}\rangle\langle\mathbf{m}|_R\,. \quad \text{(B5)}$$

The cross-entropy will then have the following representation

$$\chi_C = \frac{\sum_{\mathbf{m}} p^\rho_{\mathbf{m}}p^\sigma_{\mathbf{m}}}{\sum_{\mathbf{m}}(p^\sigma_{\mathbf{m}})^2} = \frac{\mathrm{tr}\,\rho_R\sigma_R}{\mathrm{tr}\,\sigma_R^2}, \quad \text{(B6)}$$

where ρ_R is the reduced state of ρ_{QR} on R, and similarly for σ_R.

We now focus on the case where ρ and σ are both stabilizer states and the circuit is a Clifford circuit, so that $\rho_{QR},\sigma_{QR},\rho_R,\sigma_R$ are all stabilizer states. Moreover, we will choose the state ρ to be obtainable from σ via erasure and dephasing channels. Equivalently, we choose states ρ and σ such that the stabilizer group $\mathcal{S}_\rho$ is a subgroup of $\mathcal{S}_\sigma$. Whenever this condition is satisfied for the initial state, it follows that $\mathcal{S}_{\rho_{QR}}\subseteq\mathcal{S}_{\sigma_{QR}}$ and $\mathcal{S}_{\rho_R}\subseteq\mathcal{S}_{\sigma_R}$ at any point of the purified circuit evolution. With this property, Eq. (B6) can be greatly simplified. We have

$$\rho_R = \frac{1}{2^{|R|}}\sum_{g\in\mathcal{S}_{\rho_R}} g, \quad \sigma_R = \frac{1}{2^{|R|}}\sum_{h\in\mathcal{S}_{\sigma_R}} h, \quad \text{(B7)}$$

[6] To see this, it is sufficient to consider the case of one qubit and one register. Initially, let the qubit be in the state $|\psi\rangle=\alpha|0\rangle+\beta|1\rangle$, and the register be in the state $|0\rangle$, so the joint state is

$$\rho_{QR} = |\psi\rangle\langle\psi|_Q\otimes|0\rangle\langle0|_R\,. \quad \text{(B1)}$$

After the CNOT cate, we have

$$\rho'_{QR} = \mathrm{CNOT}_{Q\to R}\cdot\rho_{QR}\cdot\mathrm{CNOT}_{Q\to R} = (\alpha|00\rangle+\beta|11\rangle)(\alpha^*\langle00|+\beta^*\langle11|)_{QR}\,. \quad \text{(B2)}$$

Under the dephasing channel on R,

$$\rho''_{QR} = \frac{1}{2}\left(\rho'_{QR}+Z_R\rho'_{QR}Z_R\right) = |\alpha|^2|0\rangle\langle0|_Q\otimes|0\rangle\langle0|_R+|\beta|^2|1\rangle\langle1|_Q\otimes|1\rangle\langle1|_R = (P_0|\psi\rangle\langle\psi|P_0)_Q\otimes|0\rangle\langle0|_R+(P_1|\psi\rangle\langle\psi|P_1)_Q\otimes|1\rangle\langle1|_R\,. \quad \text{(B3)}$$

The result ρ''_{QR} is a mixture of different trajectories, with the measurement outcome stored in R. Generalization to many qubits and many registers can be carried out in a similar fashion.

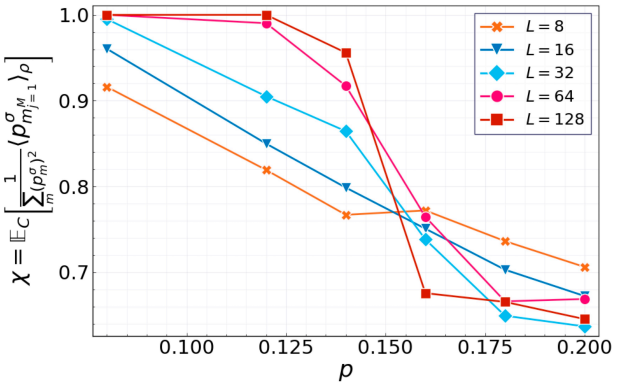

FIG. 5. Numerical results of χ for initial states $\rho = (|0\rangle\langle 0|)^{\otimes L/2} \otimes (|+\rangle\langle +|)^{\otimes L/2}$ and $\sigma = (|0\rangle\langle 0|)^{\otimes L}$, following the procedure in Eq. (11). Despite a different choice of initial state, the results are comparable to Fig. 2(a) and Fig. 3. Here the number of circuit realizations is 300, and for each circuit $M = 100$ shots of the circuit are taken.

and

$$\begin{aligned} \mathrm{tr}\,\rho_R\sigma_R &= \frac{1}{2^{2|R|}} \sum_{g\in\mathcal{S}_{\rho_R}} \sum_{h\in\mathcal{S}_{\sigma_R}} \mathrm{tr}\, gh \\ &= \frac{1}{2^{2|R|}} \sum_{g\in\mathcal{S}_{\rho_R}} \sum_{h\in\mathcal{S}_{\rho_R}} \mathrm{tr}\, gh \\ &= \mathrm{tr}\,\rho_R^2. \end{aligned} \tag{B8}$$

Here, we noticed that $\mathrm{tr}\, gh = 2^{|R|}\delta_{gh}$ for Pauli strings g and h, and used $\mathcal{S}_{\rho_R} \subseteq \mathcal{S}_{\sigma_R}$. Thus, the cross-entropy is simply the ratio between the second Renyi purity of the probability distributions $\{p^\rho_{\mathbf{m}}\}$ and $\{p^\sigma_{\mathbf{m}}\}$,

$$\chi_C = \frac{\mathrm{tr}\,\rho_R^2}{\mathrm{tr}\,\sigma_R^2} = \frac{\sum_{\mathbf{m}} \left(p^\rho_{\mathbf{m}}\right)^2}{\sum_{\mathbf{m}} \left(p^\sigma_{\mathbf{m}}\right)^2}. \tag{B9}$$

For Clifford circuit evolution, the second Renyi purity equals $2^{-N_{\mathrm{rand}}}$, where N_{rand} is the number of measurements (out of the total N) whose outcome is randomly ± 1 (see footnote 2). This number N_{rand} can be obtained by running the circuit once for each initial state [45]. We have

$$\chi_C = 2^{-N_{\mathrm{rand}}(C,\rho)+N_{\mathrm{rand}}(C,\sigma)}. \tag{B10}$$

More generally, for initial states ρ and σ that may not satisfy the condition $\mathcal{S}_\rho \subseteq \mathcal{S}_\sigma$, Eq. (B8) takes the form

$$\mathrm{tr}\,\rho_R\sigma_R = \frac{1}{2^{2|R|}} \sum_{g\in\mathcal{S}_{\rho_R}} \sum_{h\in\mathcal{S}_{\sigma_R}} \mathrm{tr}\, gh = \frac{|\mathcal{S}_{\rho_R} \cap \mathcal{S}_{\sigma_R}|}{2^{|R|}}. \tag{B11}$$

Computing $|\mathcal{S}_{\rho_R} \cap \mathcal{S}_{\sigma_R}|$ without further simplifications can take time $O(L^3 \cdot T^3)$. In practice it would be most convenient to carry out the sampling procedure outlined at the beginning of Sec. II B, which, as we have shown, converges in poly$(1/\varepsilon)$ time. So we can use the procedure in Eq. (11),

$$\chi_C = \lim_{M\to\infty} \left\langle \frac{p^\sigma_{\mathbf{m}_{j=1}^M}}{\sum_{\mathbf{m}} \left(p^\sigma_{\mathbf{m}}\right)^2} \right\rangle_\rho. \tag{B12}$$

That is, we run the ρ-circuit and obtain an ensemble of measurement histories $\{\mathbf{m}_j\}$, and take the average of their corresponding probabilities $p^\sigma_{\mathbf{m}_j}$ in the σ-circuit, divided by $\sum_{\mathbf{m}} \left(p^\sigma_{\mathbf{m}}\right)^2 = 2^{-N_{\mathrm{rand}}}$. Each $p^\sigma_{\mathbf{m}_j} / \sum_{\mathbf{m}} \left(p^\sigma_{\mathbf{m}}\right)^2$ can be computed in polynomial time by running a σ-circuit in parallel.

To verify the validity of this method, we consider initial states $\rho = (|0\rangle\langle 0|)^{\otimes L/2} \otimes (|+\rangle\langle +|)^{\otimes L/2}$ and $\sigma = (|0\rangle\langle 0|)^{\otimes L}$. Both are stabilizer states, but $\mathcal{S}_\rho \not\subseteq \mathcal{S}_\sigma$, and Eq. (B10) does not apply. We carry out the sampling procedure in Eq. (11), and plot the results in Fig. 5, which we find comparable to Fig. 2(a) despite a more involved numerical calculation. Thus, to estimate χ we have the freedom of choosing ρ, as consistent with the picture developed in Appendix A.

Appendix C: Bitstring distribution in the output state

As we discussed in the main text, the linear cross-entropy χ for the MIPT is most conveniently estimated numerically for Clifford circuits with a stabilizer initial state ρ, and can be extended to Clifford circuit with a non-stabilizer ρ (and scaled up) given access to a quantum processor. In either case χ admits the same interpretation in the stat mech language, and should contain the same universal data, e.g. the critical exponent ν. Thus, one natural question is whether considering a non-stabilizer initial state on a quantum processor reveals anything new about the physics surrounding the MIPT.

As we have shown, in the volume law phase, $\chi = 1$ almost identically for sufficiently large L; and it follows that it is impossible – in an information-theoretic sense – to distinguish two different initial states from infrequent ($p < p_c$) bulk measurements. The information about the initial state must therefore be contained in the output state of the circuit.

The difference between the two initial states may be detected using various measures [60, 61]. Here we consider the probability distribution over bitstrings when each qubit of the output state of the ρ-circuit (namely $\rho_{\mathbf{m}} = C_{\mathbf{m}}\rho C^\dagger_{\mathbf{m}}$ in Eq. (1)) is measured in the computational basis, where the input state ρ is taken to be the one from Eq. (13). For a fixed bitstring $x \in \{0,1\}^L$, the probability for this outcome to occur in the output state of $C_{\mathbf{m}}$ is

$$\mu(x; C_{\mathbf{m}}, \rho) = \langle x|\, \overline{\rho}_{\mathbf{m}}\, |x\rangle\,, \tag{C1}$$

where $\overline{\rho}_{\mathbf{m}} = \rho_{\mathbf{m}} / \mathrm{tr}\,\rho_{\mathbf{m}}$ is the normalized output state. In Fig. 6(a) we plot the fraction of bistrings with probability

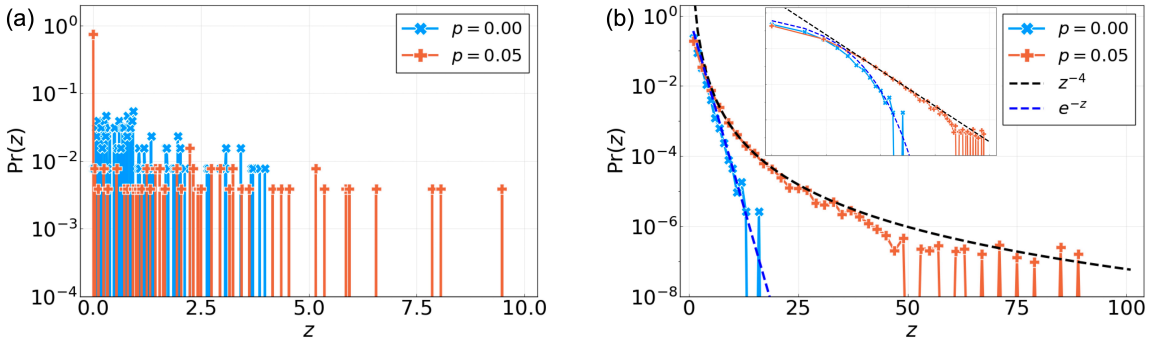

FIG. 6. (a) The bitstring distribution defined in Eq. (C2), for a typical instance of $C_{\mathbf{m}}$ with a generic (nonstabilizer) initial state ρ in Eq. (13). We see a broad distribution, in sharp contrast to the bitstring distribution from a stabilizer initial state in Eq. (C3). (b) The bitstring distribution defined in Eq. (C4), when the data in (a) is averaged over $C_{\mathbf{m}}$. The Porter-Thomas distribution $\Pr(z) = e^{-z}$ is reproduced in the unitary limit $p = 0$, and a qualitatively different (powerlaw) distribution is observed for $p > 0$ (see Eq. (C6)).

$\mu = z/D$ in a typical instance of $C_{\mathbf{m}}$, where z is a random variable and $D = 2^L$ is the dimension of the L-qubit Hilbert space,

$$\Pr(z; C_{\mathbf{m}}, \rho) = \frac{1}{D} \sum_{x\in\{0,1\}^L} \delta(z - \mu(x; C_{\mathbf{m}}, \rho) \cdot D). \quad \text{(C2)}$$

As we can see, in a typical circuit at $p > 0$ the output distribution is already notably broader than at $p = 0$.

On the other hand, for the output of the σ-circuit, namely $\overline{\sigma}_{\mathbf{m}} = C_{\mathbf{m}}\sigma C_{\mathbf{m}}^\dagger / \operatorname{tr} C_{\mathbf{m}}\sigma C_{\mathbf{m}}^\dagger$ where σ is a stabilizer state, the distribution function $\Pr(z; C_{\mathbf{m}}, \sigma)$ is much simpler:

$$\Pr(z; C_{\mathbf{m}}, \sigma) = \left(1 - \frac{1}{2^{L-n}}\right)\delta(z) + \frac{1}{2^{L-n}}\delta(z - 2^{L-n}). \quad \text{(C3)}$$

Here, n is an integer between 0 and L. The broad distribution in Fig. 6(a) is markedly different from this, and is due to the fact that ρ is a non-stabilizer state.

We focus on the non-stabilizer state $\overline{\rho}_{\mathbf{m}}$ henceforth. In analogy with random unitary circuits, we consider the circuit average of $\Pr(z; C_{\mathbf{m}})$,

$$\begin{aligned}\Pr(z) &:= \mathbb{E}_{C_{\mathbf{m}}} \Pr(z; C_{\mathbf{m}}) \\ &= \frac{1}{D} \sum_{x\in\{0,1\}^L} \mathbb{E}_{C_{\mathbf{m}}} \delta(z - \mu(x; C_{\mathbf{m}}, \rho) \cdot D) \\ &= \mathbb{E}_{C_{\mathbf{m}}} \delta(z - \mu(x; C_{\mathbf{m}}, \rho) \cdot D). \end{aligned} \quad \text{(C4)}$$

Here, after circuit averaging $\Pr(z)$ does not depend on the bitstring x despite the notation, and we can choose $|x\rangle = |0\rangle^{\otimes L}$, for concreteness.

In the unitary limit $p = 0$, there are no measurements, and $\mathbb{E}_{C_{\mathbf{m}}} = \mathbb{E}_U$. Here $\Pr(z)$ should be the Porter-Thomas distribution since the Clifford group forms a unitary 2-design,

$$\Pr(z) = \mathbb{E}_U \delta(z - \mu(x; U, \rho) \cdot D) = e^{-z}. \quad \text{(C5)}$$

For $p > 0$, we observe numerically that (see Fig. 6(b))

$$\Pr(z) \propto \alpha\delta(z) + \beta z^{-\gamma}, \quad \gamma \approx 4. \quad \text{(C6)}$$

Since this function $z^{-\gamma}$ diverges as $z \to 0$, the asymptotics is only valid for z greater than some (possibly L-dependent, see below) cutoff λ. We suspect that the exponent γ is universal (as we have checked for a few values of p), while the constants of proportionality α, β are λ-dependent (to keep $\Pr(z)$ normalized) and nonuniversal.

Since the distributions in Fig. 6(a,b) have long tails – meaning that in a given $C_{\mathbf{m}}$ the bitstrings occur with rather uneven probabilities – predicting which ones occur more commonly should be hard, and it is tempting to conjecture the classical hardness of sampling x from the probability distribution $\mu(x; C_{\mathbf{m}}, \rho)$, for a generic (nonstabilizer) initial state ρ. Given that on a noiseless quantum computer we can simulate the hybrid circuit and produce the state $\rho_{\mathbf{m}}$, such hybrid circuits may serve the purpose of demonstrating quantum advantage.

However, there is an important caveat here. As evident from the definition of μ, for a fixed C the bitstring distribution as obtained from measuring $\rho_{\mathbf{m}}$ still has an explicit dependence on $\mathbf{m}$. In each run of the circuit, one gets a new $\mathbf{m}$, and the bitstring distribution μ changes from run to run. Thus, even the circuit itself cannot effiently sample $\mu(x; C_{\mathbf{m}}, \rho)$ for any given $\mathbf{m}$, for we have no control over $\mathbf{m}$, and cannot repeatedly prepare $\rho_{\mathbf{m}}$. To sample x from $\mu(x; C_{\mathbf{m}}, \rho)$ for a given $\mathbf{m}$, it seems that we must again resort to postselection.

It might be possible to avoid the need of postselection by focusing on a particular subset of non-stabilizer initial states ρ, for which the bitstring distributions $\mu(x; C_{\mathbf{m}}, \rho)$ for different $\mathbf{m}$ can be related to each other by a change of variable in x. Characterizations of such ρ is beyond the scope of this work, which we will discuss elsewhere.